 doi:10.20944/preprints202209.0319.v1

Article

Calcium-bound S100P Protein is a Promiscuous Binding Partner of the Four-Helical Cytokines

Alexey S. Kazakov [1], Evgenia I. Deryusheva [1], Maria E. Permyakova [1], Andrey S. Sokolov [1], Victoria A. Rastrygina [1], Vladimir N. Uversky [1,2,*], Eugene A. Permyakov [1], and Sergei E. Permyakov [1,*]

[1] Institute for Biological Instrumentation, Pushchino Scientific Center for Biological Research of the Russian Academy of Sciences, Institutskaya str., 7, Pushchino, Moscow Region 142290, Russia; fenixfly@yandex.ru (A.S.K.); janed1986@ya.ru (E.I.D.); mperm1977@gmail.com (M.E.P.); 212sok@gmail.com (A.S.S.); certusfides@gmail.com (V.A.R.); epermyak@yandex.ru (E.A.P.); permyakov.s@gmail.com (S.E.P.)

[2] Department of Molecular Medicine and USF Health Byrd Alzheimer's Research Institute, Morsani College of Medicine, University of South Florida, Tampa, FL 33612, USA; vuversky@usf.edu (V.N.U.)

* Correspondence: vuversky@usf.edu (V.N.U.); permyakov.s@gmail.com (S.E.P.); Tel.: +7-(495)-143-7740 (S.E.P.); Fax: +7-(4967)-33-05-22 (S.E.P.)

Abstract: S100 proteins are multifunctional calcium-binding proteins of vertebrates that act intracellularly, extracellularly, or both, and are engaged in the progression of many socially significant diseases. Their extracellular action is typically mediated by the recognition of specific receptor proteins. Besides, recent studies indicate the ability of some S100 proteins to affect cytokine signaling through direct interaction with cytokines. S100P was shown to be the S100 protein most actively involved in interactions with some of four-helical cytokines. To assess selectivity of S100P protein binding to four-helical cytokines, we have probed interaction of Ca2+-bound recombinant human S100P with a panel of 32 four-helical human cytokines covering all structural families of this fold, using surface plasmon resonance spectroscopy. 22 cytokines from all families of four-helical cytokines are S100P binders with the equilibrium dissociation constants, Kd, ranging from 1 nM to 3 μM (below the Kd value for the S100P complex with the V domain of its conventional receptor, receptor for advanced glycation end products, RAGE). Molecular docking and mutagenesis studies revealed the presence in the S100P molecule of a cytokine-binding site, which overlaps with the RAGE-binding site. Since S100 binding to four-helical cytokines inhibits their signaling in some cases, the revealed ability of S100P protein to interact with ca 71% of the four-helical cytokines indicates that S100P may serve as a poorly selective inhibitor of their action.

Keywords: cytokine; S100 protein; S100P; protein–protein interaction

1. Introduction

S100 proteins (reviewed in ref. [1-3]) are the most representative family of the Ca^{2+}-binding proteins of the EF-hand superfamily, defined by the presence of a Ca^{2+}-binding motif called the 'EF-hand' [4]: a 12-residue Ca^{2+}-binding loop flanked by two α-helices (PROSITE [5] entry PDOC00018). Evolutionary, first S100 proteins (including S100P) emerged nearly 500 million years ago and are encountered exclusively in vertebrates [6]. Human S100 protein family includes 21 members (79-114 residues; excluding S100 fused-type proteins), comprised of an atypical low-affinity N-terminal EF-hand and a classical high-affinity C-terminal EF-hand motif connected via a flexible 'hinge' region [7]. With the exception of monomeric S100G, S100 proteins are considered (homo/hetero)dimeric, and some of them may form higher order oligomers [2,8]. Some S100 proteins possess Zn^{2+}/Cu^{2+}/Mn^{2+}-binding sites [7,9] and undergo post-translational modifications [2,3]. The tissue/cell-specific expression of S100 proteins, their ability to localize in cytosol, nucleus, and extracellular space, and the capability to interact with a wide spectrum of targets (proteins, including receptor/membrane proteins, lipids, and nucleic acids) also contrib-

Preprints (www.preprints.org) | NOT PEER-REVIEWED | Posted: 21 September 2022 doi:10.20944/preprints202209.0319.v1

ute to their multifunctionality [1,2,10]. Despite their structural similarity, each of S100 proteins is functionally unique. Some of them are associated with cancer, inflammatory, autoimmune, cardiovascular, pulmonary and neurodegenerative diseases, which makes them attractive diagnostic and therapeutic targets [11-17]. Upon release into extracellular space, some S100 proteins act similarly to cytokines in an autocrine/paracrine manner via recognition of cell surface receptors, including RAGE, TLR4, ErbB1, ErbB3, ErbB4, CD36, CD68, CD147, CD166, neuroplastin-β, 5-HT_{1B}, IL-10R and SIRL-1 [2,10,18]. Furthermore, some of the extracellular S100 proteins are able to influence cytokine signaling via their direct binding; e.g., S100A1/A4/A6/B/P bind to IFN-β [10,19,20], distinct subsets of S100A1/A6/B/P interact with IL-6 family cytokines IL-11, OSM, CNTF, CT-1, and CLCF1 [21], S100A2/A6/P bind EPO [22], S100A4 binds to ErbB1 ligands [23], S100A13 interacts with IL1α/FGF1 [24,25], S100B binds FGF2 [26]. Some of the S100-cytokine interactions could favor non-canonical secretion of the both interaction partners, as was shown for S100A13 - IL1α/FGF1 [24,25].

It should be noted, that most of the S100-cytokine interactions correspond to the four-helical cytokines, IFN-β, representatives of IL-6 family cytokines, and EPO. Among the cytokine-specific proteins, S100P recognizes the maximal number of the cytokines (see **Table 1**), indicating its poor selectivity towards the four-helical cytokines. To elucidate selectivity of S100P protein binding to four-helical cytokines, in the present work we probed interaction of Ca^{2+}-loaded S100P with a panel of 32 four-helical cytokines covering all their structural families, including "Short-chain cytokines" (SCOP [27] ID 4000852), "Long-chain cytokines" (SCOP ID 4000851), and "Interferons/interleukin-10 (IL-10)" (SCOP ID 4000854) (**Table 2**).

Table 1. The literature data on parameters of the heterogeneous ligand model (1), describing the SPR data on kinetics of interaction between Ca2+-loaded S100P and four-helical cytokines (cytokine immobilization on the sensor chip surface by amine coupling).

Cytokine	K_{d1}, M	K_{d2}, M	Reference
Short-chain cytokines			
EPO	$(5.4 \pm 1.2) \times 10^{-7}$	$(1.8 \pm 0.5) \times 10^{-6}$	[22]
Long-chain cytokines			
IL-11	$(3.2 \pm 0.3) \times 10^{-8}$	$(2.88 \pm 0.01) \times 10^{-7}$	[28]
Cardiotrophin-like cytokine factor 1	$(8.1 \pm 2.6) \times 10^{-8}$	$(1.4 \pm 0.8) \times 10^{-7}$	[21]
Ciliary neurotrophic factor	$(1.0 \pm 0.6) \times 10^{-7}$	$(1.1 \pm 0.8) \times 10^{-7}$	[21]
Cardiotrophin-1	$(1.9 \pm 0.5) \times 10^{-8}$	$(9.8 \pm 2.7) \times 10^{-7}$	[21]
Oncostatin-M	$(7.0 \pm 4.2) \times 10^{-7}$	$(2.0 \pm 0.9) \times 10^{-6}$	[21]
Interferons/IL-10			
IFN-β	$(5.34 \pm 0.10) \times 10^{-8}$	$(6.1 \pm 2.3) \times 10^{-7}$	[10]

2. Results and Discussion

2.1. S100P interaction with specific four-helical cytokines

To probe the selectivity of S100P binding to four-helical cytokines, 32 cytokines covering all families of this fold (**Table 2**) were immobilized on the surface of the SPR sensor chip by amine coupling, and 62 nM - 16 μM solutions of Ca^{2+}-loaded (1 mM $CaCl_2$) recombinant human S100P were passed over the chip at 25ºC. 10 cytokines indicated in **Table S1** did not reveal specificity to S100P (data not shown). Meanwhile, the SPR sensograms for 22 cytokines exhibited the S100P concentration-dependent effects (**Figures 1-3**). The dissociation phases of the sensograms are biphasic revealing the existence of a relatively fast process and a much slower process. Meanwhile, the SPR sensograms for 22 cytokines exhibited the S100P concentration-dependent effects (**Figures 1-3**).

Table 2. The four-helical cytokine samples studied in the present work with regard to their affinity to Ca^{2+}-bound S100P.

Preprints (www.preprints.org) | NOT PEER-REVIEWED | Posted: 21 September 2022 doi:10.20944/preprints202209.0319.v1

Full name	Abbreviation	UniProt ID	Manufacturer	Cat. number	Source
Short-chain cytokines					
Macrophage colony-stimulating factor 1	M-CSF	P09603	PeproTech	300-25	*E.coli*
Granulocyte-macrophage colony-stimulating factor	GM-CSF	P04141	PeproTech	300-03	*E.coli*
Interleukin-2	IL-2	P60568	PeproTech	AF-200-02	*E.coli*
Interleukin-3	IL-3	P08700	SCI-Store (Russia)	PSG160-10	CHO
Interleukin-4	IL-4	P05112	PeproTech	AF-200-04	*E.coli*
Interleukin-5	IL-5	P05113	PeproTech	200-05	*E.coli*
Interleukin-9	IL-9	P15248	PeproTech	200-09	*E.coli*
Interleukin-13	IL-13	P35225	PeproTech	200-13	*E.coli*
Interleukin-15	IL-15	P40933	PeproTech	200-15	*E.coli*
Interleukin-21	IL-21	Q9HBE4	PeproTech	200-21	*E.coli*
Thrombopoietin	THPO	P40225	SCI-Store (Russia)	PSG090-10	CHO
Long-chain cytokines					
Interleukin-7	IL-7	P13232	SCI-Store (Russia)	PSG240-10	CHO
Interleukin-31	IL-31	Q6EBC2	PeproTech	200-31	*E.coli*
Granulocyte colony-stimulating factor	G-CSF	P09919	Pharmstandard (Russia)	n/a	*E.coli*
Somatotropin	GH	P01241	PeproTech	AF-100-40	*E.coli*
Growth hormone variant	GH-V	P01242	R&D Systems	7668-GH/CF	*E.coli*
Prolactin	PRL	P01236	PeproTech	100-07	*E.coli*
Leptin	LEP	P41159	PeproTech	AF-300-27	*E.coli*
Thymic stromal lymphopoietin	TSLP	Q969D9	PeproTech	300-62	*E.coli*
Chorionic somatomammotropin hormone 1	PL	P0DML2	R&D Systems	5757-PL/CF	CHO
Interleukin-12	IL-12	P29459* & P29460	PeproTech	200-12H	HEK293
Interleukin-23	IL-23	Q9NPF7* & P29460	PeproTech	200-23	Hi-5
Interleukin-27	IL-27	Q8NEV9* & Q14213	PeproTech	200-38	HEK293
Interleukin-35	IL-35	P29459* & Q14213	PeproTech	200-37	HEK293
Interferons/IL-10					
Interleukin-10	IL-10	P22301	PeproTech	AF-200-10	*E.coli*
Interleukin-20	IL-20	Q9NYY1	PeproTech	200-20	*E.coli*
Interleukin-22	IL-22	Q9GZX6	PeproTech	200-22	*E.coli*
Interleukin-24	IL-24	Q13007	PeproTech	200-35	CHO
Interleukin-26	IL-26	Q9NPH9	R&D Systems	1375-IL/CF	*E.coli*
Interferon α-2	IFN-α2	P01563	Vector-Medica (Russia)	n/a	*E.coli*
Interferon γ	IFN-γ	P01579	Pharmaclon (Russia)	n/a	*E.coli*
Interferon ω-1	IFN-ω1	P05000	PeproTech	300-02J	*E.coli*

* denotes the chain used for SCOP 2 [27] family assignment
n/a, not applicable

The dissociation phases of the sensograms are biphasic revealing the existence of a relatively fast process and a much slower process. The both processes are adequately described within the heterogeneous ligand model (1) (**Figures 1-3**, **Table 3**), which was previously successfully used for description of the S100-cytokine interactions [10,19-22,28,29]. The SPR data for IL-13 are described by the one-site binding scheme. The lowest equilibrium dissociation constants, K_d, range from 1 nM (THPO) to 3 μM (IL-10) (**Table 3**), which is below the K_d value of 6 μM found earlier for the complex of Ca^{2+}-bound S100P with the V domain of its receptor, RAGE [30].

Preprints (www.preprints.org) | NOT PEER-REVIEWED | Posted: 21 September 2022 doi:10.20944/preprints202209.0319.v1

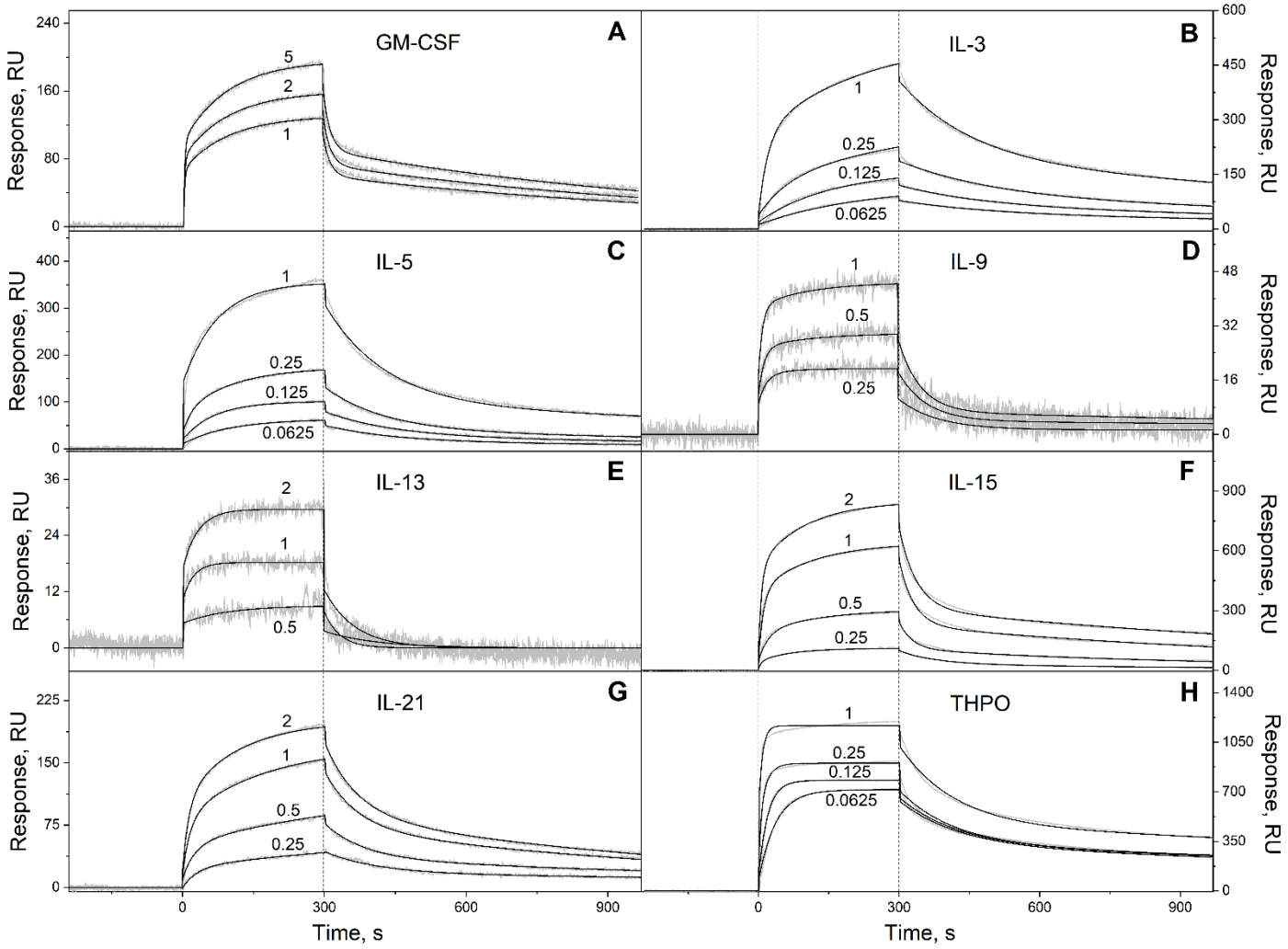

Figure 1. Kinetics of the interaction of Ca^{2+}-loaded S100P with specific short-chain four-helical cytokines shown in **Table 2** at 25°C, monitored by SPR spectroscopy using S100P as an analyte and the cytokines as a ligand immobilized on the sensor chip surface by amine coupling. Buffer conditions: 10 mM HEPES, 150 mM NaCl, 1 mM $CaCl_2$, 0.05% TWEEN 20, pH 7.4. The vertical dotted lines mark the association phase, followed by the dissociation phase. Molar analyte concentrations (μM) are indicated for the sensograms. The grey curves are experimental, while the black curves are theoretical, calculated according to the *heterogeneous ligand* model (1) or one-site binding model, in the case of IL-13 (see **Table 3**).

Preprints (www.preprints.org) | NOT PEER-REVIEWED | Posted: 21 September 2022 doi:10.20944/preprints202209.0319.v1

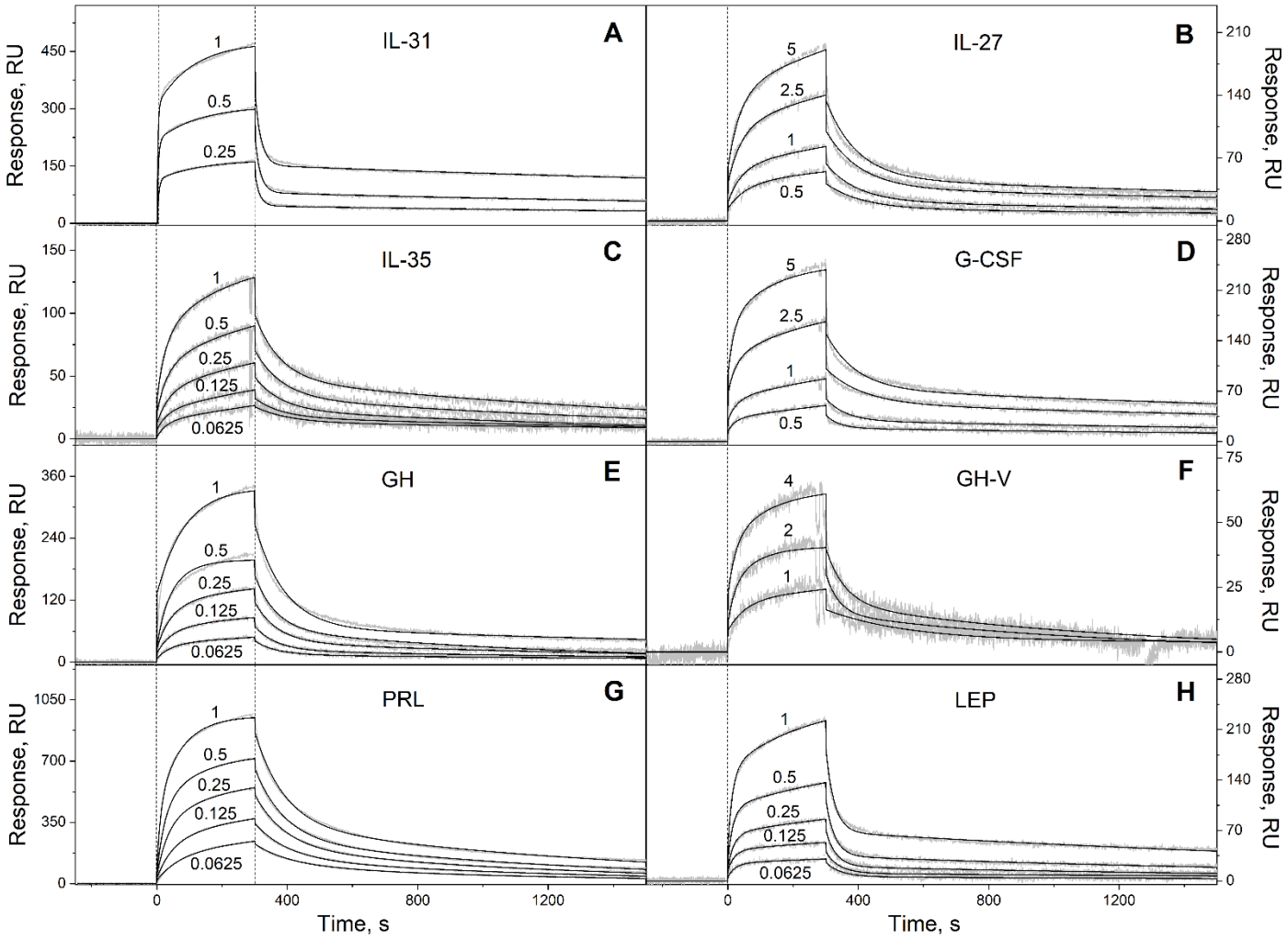

Figure 2. Kinetics of the interaction of Ca^{2+}-loaded S100P with specific long-chain four-helical cytokines shown in **Table 2** at 25°C, monitored by SPR spectroscopy using S100P as an analyte and the cytokines as a ligand immobilized on the sensor chip surface by amine coupling. Buffer conditions: 10 mM HEPES, 150 mM NaCl, 1 mM $CaCl_2$, 0.05% TWEEN 20, pH 7.4. The vertical dotted lines mark the association phase, followed by the dissociation phase. Molar analyte concentrations (μM) are indicated for the sensograms. The grey curves are experimental, while the black curves are theoretical, calculated according to the *heterogeneous ligand* model (1) (see **Table 3**).

Preprints (www.preprints.org) | NOT PEER-REVIEWED | Posted: 21 September 2022 doi:10.20944/preprints202209.0319.v1

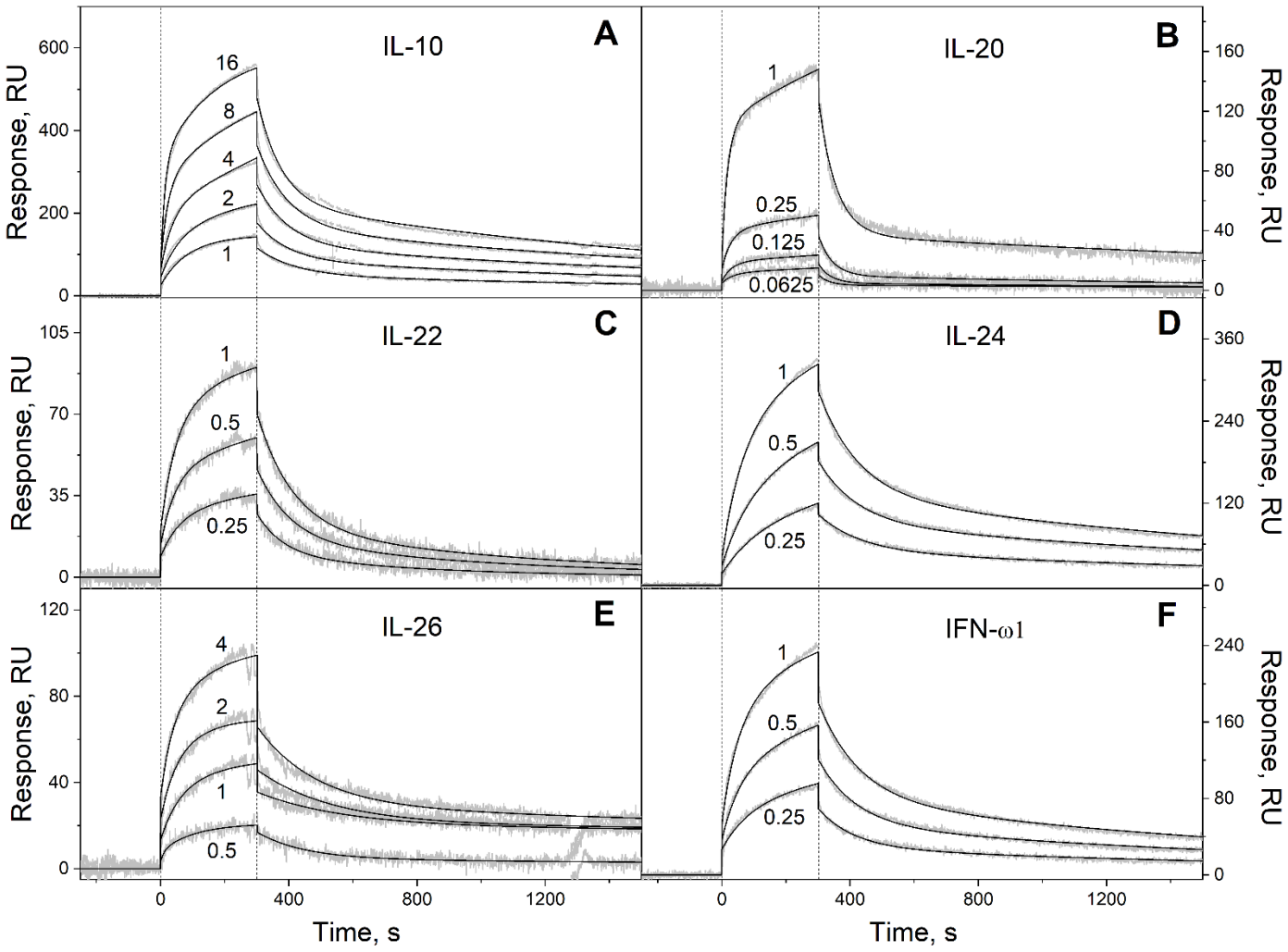

Figure 3. Kinetics of the interaction of Ca^{2+}-loaded S100P with specific four-helical cytokines of Interferons/IL-10 family shown in **Table 2** at 25°C, monitored by SPR spectroscopy using S100P as an analyte and the cytokines as a ligand immobilized on the sensor chip surface by amine coupling. Buffer conditions: 10 mM HEPES, 150 mM NaCl, 1 mM $CaCl_2$, 0.05% TWEEN 20, pH 7.4. The vertical dotted lines mark the association phase, followed by the dissociation phase. Molar analyte concentrations (μM) are indicated for the sensograms. The grey curves are experimental, while the black curves are theoretical, calculated according to the *heterogeneous ligand* model (1) (see **Table 3**).

Preprints (www.preprints.org) | NOT PEER-REVIEWED | Posted: 21 September 2022 doi:10.20944/preprints202209.0319.v1

Table 3. Parameters of the *heterogeneous ligand* model (1), describing the SPR data on kinetics of interaction between Ca^{2+}-loaded S100P and specific four-helical cytokines shown in **Table 2** at 25°C (see **Figures 1-3**).

Cytokine	k_{d1}, s^{-1}	K_{d1}, M	k_{d2}, s^{-1}	K_{d2}, M
Short-chain cytokines				
GM-CSF	$(1.13 \pm 0.23) \times 10^{-3}$	$(2.45 \pm 1.45) \times 10^{-7}$	$(6.72 \pm 2.13) \times 10^{-2}$	$(4.50 \pm 1.75) \times 10^{-7}$
IL-3	$(6.27 \pm 0.38) \times 10^{-4}$	$(2.32 \pm 0.81) \times 10^{-8}$	$(5.29 \pm 0.86) \times 10^{-3}$	$(5.79 \pm 2.19) \times 10^{-7}$
IL-5	$(6.12 \pm 1.12) \times 10^{-4}$	$(3.66 \pm 1.13) \times 10^{-9}$	$(7.12 \pm 0.77) \times 10^{-3}$	$(8.33 \pm 3.58) \times 10^{-7}$
IL-9	$(5.31 \pm 1.69) \times 10^{-4}$	$(3.47 \pm 2.66) \times 10^{-8}$	$(1.70 \pm 0.48) \times 10^{-2}$	$(1.36 \pm 0.78) \times 10^{-7}$
IL-13*	$(1.83 \pm 1.09) \times 10^{-2}$	$(2.30 \pm 0.44) \times 10^{-6}$	n/a	n/a
IL-15	$(1.09 \pm 0.25) \times 10^{-3}$	$(1.02 \pm 0.72) \times 10^{-7}$	$(2.72 \pm 1.03) \times 10^{-2}$	$(9.80 \pm 5.84) \times 10^{-7}$
IL-21	$(9.28 \pm 2.85) \times 10^{-4}$	$(2.72 \pm 0.43) \times 10^{-7}$	$(1.26 \pm 0.26) \times 10^{-2}$	$(2.85 \pm 1.73) \times 10^{-7}$
THPO	$(4.09 \pm 0.49) \times 10^{-4}$	$(8.34 \pm 2.79) \times 10^{-10}$	$(8.29 \pm 0.38) \times 10^{-3}$	$(4.12 \pm 2.44) \times 10^{-8}$
Long-chain cytokines				
IL-31	$(2.30 \pm 0.52) \times 10^{-4}$	$(2.52 \pm 1.30) \times 10^{-8}$	$(5.83 \pm 0.79) \times 10^{-2}$	$(2.02 \pm 1.12) \times 10^{-7}$
IL-27#	$(9.94 \pm 0.75) \times 10^{-3}$	$(8.59 \pm 2.67) \times 10^{-7}$	$(3.57 \pm 0.64) \times 10^{-4}$	$(1.69 \pm 0.59) \times 10^{-6}$
IL-35#	$(5.31 \pm 1.31) \times 10^{-4}$	$(9.62 \pm 4.92) \times 10^{-8}$	$(1.20 \pm 0.13) \times 10^{-2}$	$(2.55 \pm 1.77) \times 10^{-7}$
G-CSF	$(3.15 \pm 0.46) \times 10^{-4}$	$(2.13 \pm 0.15) \times 10^{-7}$	$(1.54 \pm 0.72) \times 10^{-2}$	$(8.54 \pm 2.80) \times 10^{-7}$
GH	$(6.69 \pm 2.77) \times 10^{-4}$	$(4.29 \pm 0.93) \times 10^{-8}$	$(1.42 \pm 0.18) \times 10^{-2}$	$(2.66 \pm 1.54) \times 10^{-7}$
GH-V	$(1.77 \pm 1.05) \times 10^{-3}$	$(1.04 \pm 0.88) \times 10^{-6}$	$(1.81 \pm 0.71) \times 10^{-2}$	$(2.73 \pm 0.15) \times 10^{-6}$
PRL	$(9.81 \pm 0.84) \times 10^{-4}$	$(5.46 \pm 2.35) \times 10^{-8}$	$(1.03 \pm 0.10) \times 10^{-2}$	$(9.06 \pm 0.17) \times 10^{-7}$
LEP	$(4.52 \pm 0.77) \times 10^{-4}$	$(1.43 \pm 0.32) \times 10^{-7}$	$(3.07 \pm 0.75) \times 10^{-2}$	$(4.04 \pm 2.35) \times 10^{-7}$
Interferons/IL-10				
IL-10	$(1.06 \pm 0.17) \times 10^{-2}$	$(2.55 \pm 0.54) \times 10^{-6}$	$(5.19 \pm 0.43) \times 10^{-4}$	$(2.66 \pm 1.68) \times 10^{-6}$
IL-20	$(4.42 \pm 0.97) \times 10^{-4}$	$(4.03 \pm 1.29) \times 10^{-7}$	$(2.46 \pm 0.51) \times 10^{-2}$	$(5.37 \pm 0.90) \times 10^{-7}$
IL-22	$(7.64 \pm 5.76) \times 10^{-3}$	$(4.82 \pm 0.96) \times 10^{-7}$	$(2.76 \pm 1.93) \times 10^{-3}$	$(7.80 \pm 0.77) \times 10^{-7}$
IL-24	$(4.83 \pm 0.21) \times 10^{-4}$	$(1.58 \pm 0.20) \times 10^{-7}$	$(7.94 \pm 0.34) \times 10^{-3}$	$(9.18 \pm 1.24) \times 10^{-7}$
IL-26	$(1.44 \pm 0.78) \times 10^{-4}$	$(9.02 \pm 4.24) \times 10^{-9}$	$(5.09 \pm 1.38) \times 10^{-3}$	$(1.32 \pm 0.24) \times 10^{-6}$
IFN-ω1	$(5.71 \pm 0.09) \times 10^{-4}$	$(1.74 \pm 0.19) \times 10^{-7}$	$(8.39 \pm 0.56) \times 10^{-3}$	$(5.78 \pm 1.18) \times 10^{-7}$

* one-site binding model is used

heterodimeric cytokines

n/a, not applicable

Examination of the free energy changes accompanying the S100P-cytokine interactions (**Figure 4**) shows that the average affinities of S100P to the cytokines belonging to the different families of four-helical cytokines decrease in the following order: short-chain cytokines > long-chain cytokines > interferons/IL-10.

Examination of the IntAct [31] and BioGRID [32] databases shows absence of the known soluble non-receptor extracellular proteins interacting with the following S100P-specific cytokines: IL-3, IL-5, IL-9, IL-13, IL-21, THPO, IL-22. Most of them belong to the family of short-chain four-helical cytokines with the highest affinity to S100P (**Figure 4A**).

It should be noted, that the S100P-specific cytokines are evolutionary distant from each other. The pairwise sequence identities within each of their SCOP families, calculated using Clustal Omega 2.1, as implemented in EMBL-EBI service [33], lie in the range from 8% to 32% (the heterodimeric cytokines were excluded). The only exception is GH - GH-V pair with the pairwise sequence identity of 93%. Therefore, the revealed S100P-cytokine interactions are mostly non-redundant.

Preprints (www.preprints.org) | NOT PEER-REVIEWED | Posted: 21 September 2022 doi:10.20944/preprints202209.0319.v1

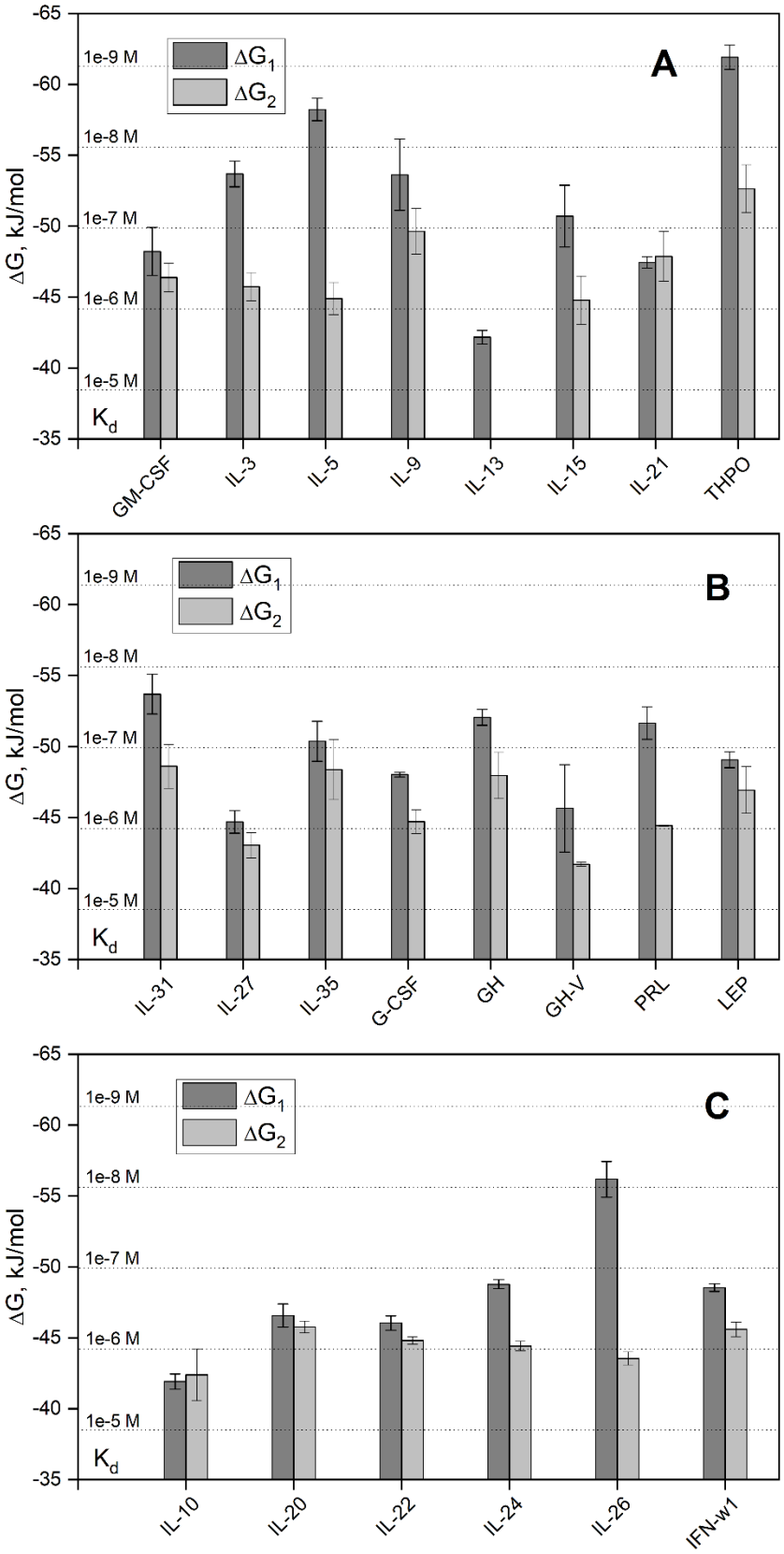

Figure 4. The free energy changes, accompanying the interaction between Ca^{2+}-loaded S100P and the four-helical cytokines of short-chain (panel **A**), long-chain (**B**) or interferons/IL-10 (**C**) families at 25°C, calculated from the SPR data shown in **Table 3**: $\Delta G_i = -RT \ln(55.3/K_{di})$, i=1,2. The scale of K_d values is indicated.

Preprints (www.preprints.org) | NOT PEER-REVIEWED | Posted: 21 September 2022 doi:10.20944/preprints202209.0319.v1

The S100P-specific cytokines (**Table 3**) coupled to SPR chip surface were readily regenerated after S100P binding upon calcium removal by passage of 20 mM EDTA solution pH 8.0 (data no shown). This fact points out the importance of the Ca^{2+}-induced structural rearrangement for the efficient S100P binding to the cytokines. Since Ca^{2+} binding mostly induces solvent exposure of S100P residues of the 'hinge' between helices α2 and α3 [29,34], this region is likely to be involved in the cytokine recognition.

Considering that the equilibrium dimer dissociation constant for Ca^{2+}-loaded S100P is about (64±24) nM [35], the SPR estimates of its affinities to the cytokines, measured at S100P concentrations from 62 nM to 16 μM (**Table 3**), mostly correspond to the dimeric state of S100P. Meanwhile, the S100P dimer dissociation constant greatly exceeds basal serum S100P level of 1 nM [36], which suggests that the serum S100P is monomeric. We have shown previously that affinities of the four-helical cytokines IL-11 and IFN-β to the monomeric S100P exceed those to its dimeric state by 1.4-2.2 orders of magnitude [10,28,37]. Hence, S100P monomerization is likely to enhance its interaction with the other four-helical cytokines. In this case, K_d values for some of the S100P-cytokine interactions (IL-3, IL-5, IL-9, THPO; IL-31, GH, PRL; IL-26) may reach subnanomolar level or less (**Figure 4**), which is enough for efficient cytokine binding to S100P at its basal serum level of 1 nM [36]. Furthermore, the blood S100P concentrations under pathological conditions may reach 5 nM [36]. Finally, the local concentrations of extracellular S100P in damaged S100P-producing tissues are expected to be even higher, thereby further promoting interactions of this protein with the four-helical cytokines.

The average blood concentrations of the most S100P-specific cytokines are normally below 0.1 nM (**Table S2**), which is significantly lower than the basal blood S100P level of 1 nM [36]. Hence, these cytokines are quantitatively unable to affect signaling of the extracellular S100P via its receptor(s). The exceptions are GH, GH-V, PRL and LEP, the average serum concentrations of which can approach the level of 1 nM or even exceed it (**Table S2**). For instance, PRL concentration in the serum of pregnant women is in the range of 3.5-17.5 nM [38]. In these cases, cytokine binding to S100P is potentially able to alter signaling of the latter. The same situation can occur under the pathological conditions accompanied by an increase in the concentrations of the S100P-specific cytokines to a (sub)nanomolar level, as observed for IL-9, IL-31, G-CSF, GH, GH-V, PRL, LEP, IL-24, IL-26 (**Table S2**).

S100P binding could modify signaling of the S100P-specific cytokines, as exemplified by inhibition of the IFN-β-induced suppression of the viability of MCF-7 breast cancer cells by S100A1/A4/B/P proteins [10,19,20]. Another opportunity is the facilitation of secretion of the S100P-specific cytokines due to the S100P binding, as previously shown for the four-helical cytokine CLCF1, which needs association with the CRLF1 for efficient secretion [39]. Similarly, S100A13 binding to cytokines IL-1α and FGF1 favors their non-canonical secretion [24,25].

The promiscuous binding of the wide spectrum of four-stranded cytokines by S100P protein under the conditions of its quantitative excess indicates the possibility that S100P serves as a buffer for the cytokines, capable of absorbing their excess when the cytokine levels are excessively increased and releasing the cytokines under conditions of their depletion.

2.2. Modeling of the S100P-cytokine complexes

To elucidate molecular determinants of the revealed interactions between Ca^{2+}-bound S100P and the wide spectrum of the four-helical cytokines (**Table 3**), models of the quaternary structures of their complexes have been built using ClusPro docking server [40] (except for the complexes with heterodimeric IL-27/IL-35). The structure of Ca^{2+}-loaded S100P dimer was extracted from its complex with V domain of RAGE (PDB entry 2MJW, **Figure 5A**). whereas the structures of the cytokines were taken from PDB (including complexes with their binding partners) or predicted using AlphaFold2 [41] (**Table S3, Figure 6**).

Preprints (www.preprints.org) | NOT PEER-REVIEWED | Posted: 21 September 2022 doi:10.20944/preprints202209.0319.v1

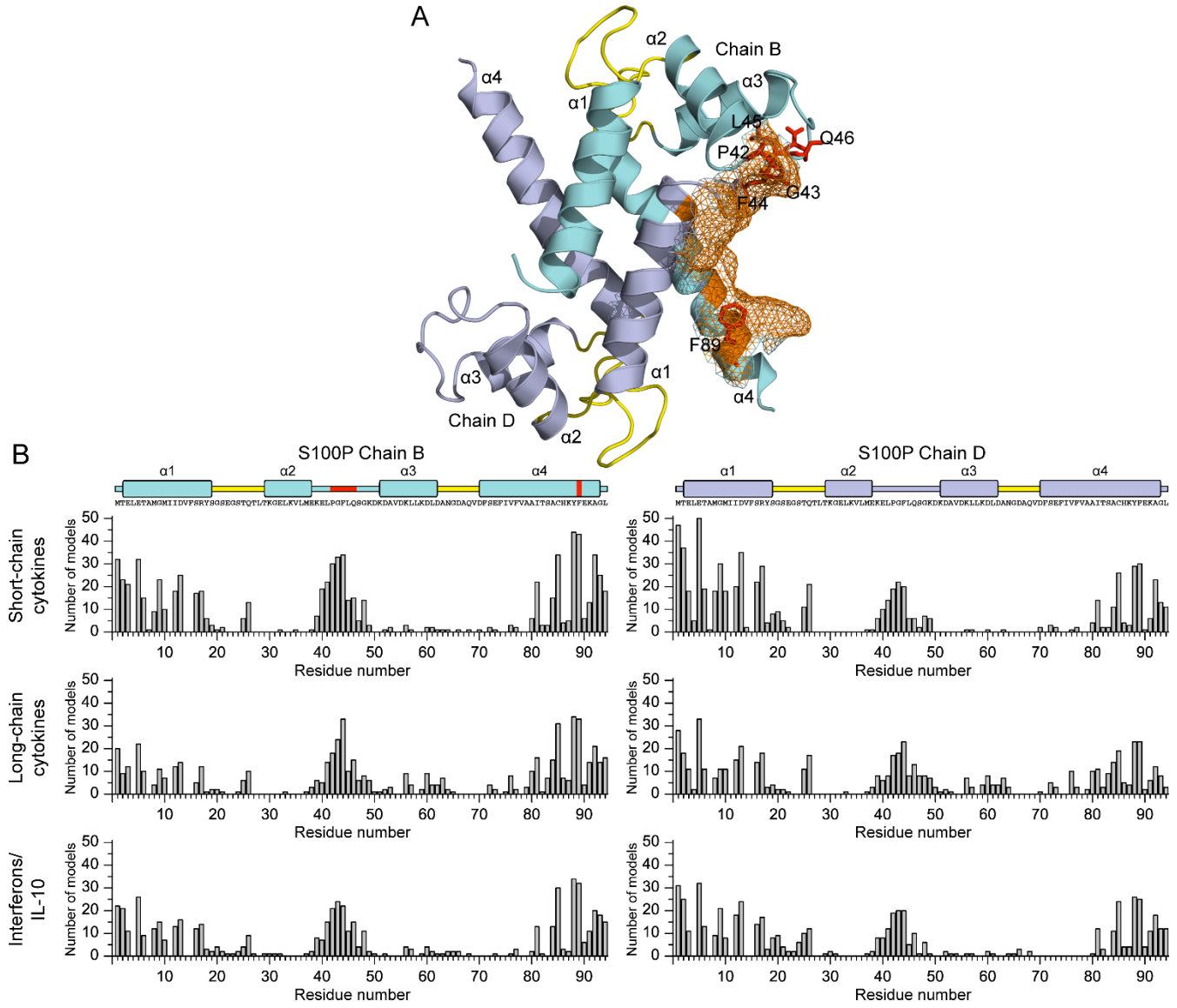

Figure 5. **A**, tertiary structure of Ca^{2+}-loaded S100P dimer (PDB entry 2MJW): chains B and D are highlighted in cyan and grey, respectively; the α-helices are labelled as α1-α4; the Ca^{2+}-binding loops are yellow-colored. The residues predicted to constitute the cytokine-binding site are shown as orange mesh surface: residues P42, G43, F44, C85, Y88, F89 (chain B) and M1, E5 (chain D). The residues P42, G43, F44, L45, Q46 and F89 (see **Table 4**) of chain B are depicted as red balls and sticks. **B**, distributions of the predicted contact residues of Ca^{2+}-loaded S100P dimer over its amino acid sequence within models of S100P complexes with representatives of specific families of four-helical cytokines (see **Table S4**). 10 docking models were taken into account for each S100P-cytokine pair. The boundaries of secondary structure elements of S100P were taken from PDB entry 2MJW; the residues P42, G43, F44, L45, Q46 and F89 (see **Table 4**) of chain B are indicated in red.

Table 4. Parameters of the heterogeneous ligand model (1), describing the SPR data on kinetics of interaction between Ca2+-loaded wild-type S100P or its mutants and the four-helical cytokines shown in **Table 3** at 25°C.

Cytokine\S100P	*Wild-type*		*F89A*		*Δ42-47*
	K_{d1}, *M*	K_{d2}, *M*	K_{d1}, *M*	K_{d1}, *M*	K_d, *M*
Short-chain cytokines					
GM-CSF	$(2.45 \pm 1.45) \times 10^{-7}$	$(4.50 \pm 1.75) \times 10^{-7}$	n.d.		n.d.

Preprints (www.preprints.org) | NOT PEER-REVIEWED | Posted: 21 September 2022 doi:10.20944/preprints202209.0319.v1

IL-3	$(2.32 \pm 0.81) \times 10^{-8}$	$(5.79 \pm 2.19) \times 10^{-7}$	n.d.		n.d.
IL-5	$(3.66 \pm 1.13) \times 10^{-9}$	$(8.33 \pm 3.58) \times 10^{-7}$	n.d.		n.d.
IL-9	$(3.47 \pm 2.66) \times 10^{-8}$	$(1.36 \pm 0.78) \times 10^{-7}$	n.d.		n.d.
IL-13*	$(2.30 \pm 0.44) \times 10^{-6}$	n/a	$>10^{-4}$		$>10^{-4}$
IL-15	$(1.02 \pm 0.72) \times 10^{-7}$	$(9.80 \pm 5.84) \times 10^{-7}$	$(1.57 \pm 0.57) \times 10^{-7}$	$(2.83 \pm 0.34) \times 10^{-7}$	$>10^{-4}$
IL-21	$(2.72 \pm 0.43) \times 10^{-7}$	$(2.85 \pm 1.73) \times 10^{-7}$	$(4.01 \pm 1.64) \times 10^{-7}$	$(9.50 \pm 4.52) \times 10^{-7}$	$>10^{-4}$
THPO	$(8.34 \pm 2.79) \times 10^{-10}$	$(4.12 \pm 2.44) \times 10^{-8}$	n.d.		n.d.
Long-chain cytokines					
IL-31	$(2.52 \pm 1.30) \times 10^{-8}$	$(2.02 \pm 1.12) \times 10^{-7}$	$(2.02 \pm 0.59) \times 10^{-7}$	$(1.18 \pm 0.53) \times 10^{-6}$	$>10^{-4}$
IL-27#	$(8.59 \pm 2.67) \times 10^{-7}$	$(1.69 \pm 0.59) \times 10^{-6}$	n.d.		n.d.
IL-35#	$(9.62 \pm 4.92) \times 10^{-8}$	$(2.55 \pm 1.77) \times 10^{-7}$	$>10^{-4}$		$>10^{-5}$
G-CSF	$(2.13 \pm 0.15) \times 10^{-7}$	$(8.54 \pm 2.80) \times 10^{-7}$	n.d.		n.d.
GH	$(4.29 \pm 0.93) \times 10^{-8}$	$(2.66 \pm 1.54) \times 10^{-7}$	$(2.92 \pm 2.66) \times 10^{-5}$	$(1.38 \pm 0.52) \times 10^{-4}$	$>10^{-4}$
GH-V	$(1.04 \pm 0.88) \times 10^{-6}$	$(2.73 \pm 0.15) \times 10^{-6}$	$>10^{-4}$		$>10^{-4}$
PRL	$(5.46 \pm 2.35) \times 10^{-8}$	$(9.06 \pm 0.17) \times 10^{-7}$	$(6.89 \pm 3.20) \times 10^{-7}$	$(3.12 \pm 0.50) \times 10^{-6}$	$>10^{-4}$
LEP	$(1.43 \pm 0.32) \times 10^{-7}$	$(4.04 \pm 2.35) \times 10^{-7}$	$(4.37 \pm 1.71) \times 10^{-6}$	$(3.57 \pm 1.77) \times 10^{-5}$	$>10^{-4}$
Interferons/IL-10					
IL-10	$(2.55 \pm 0.54) \times 10^{-6}$	$(2.66 \pm 1.68) \times 10^{-6}$	$(4.74 \pm 3.41) \times 10^{-6}$	$(6.05 \pm 1.47) \times 10^{-6}$	$>10^{-4}$
IL-20	$(4.03 \pm 1.29) \times 10^{-7}$	$(5.37 \pm 0.90) \times 10^{-7}$	n.d.		n.d.
IL-22	$(4.82 \pm 0.96) \times 10^{-7}$	$(7.80 \pm 0.77) \times 10^{-7}$	n.d.		n.d.
IL-24	$(1.58 \pm 0.20) \times 10^{-7}$	$(9.18 \pm 1.24) \times 10^{-7}$	n.d.		n.d.
IL-26	$(9.02 \pm 4.24) \times 10^{-9}$	$(1.32 \pm 0.24) \times 10^{-6}$	$>10^{-4}$		$>10^{-4}$
IFN-ω1	$(1.74 \pm 0.19) \times 10^{-7}$	$(5.78 \pm 1.18) \times 10^{-7}$	n.d.		n.d.

* one-site binding model is used

heterodimeric cytokines

n/a, not applicable

n.d., not determined

Preprints (www.preprints.org) | NOT PEER-REVIEWED | Posted: 21 September 2022 doi:10.20944/preprints202209.0319.v1

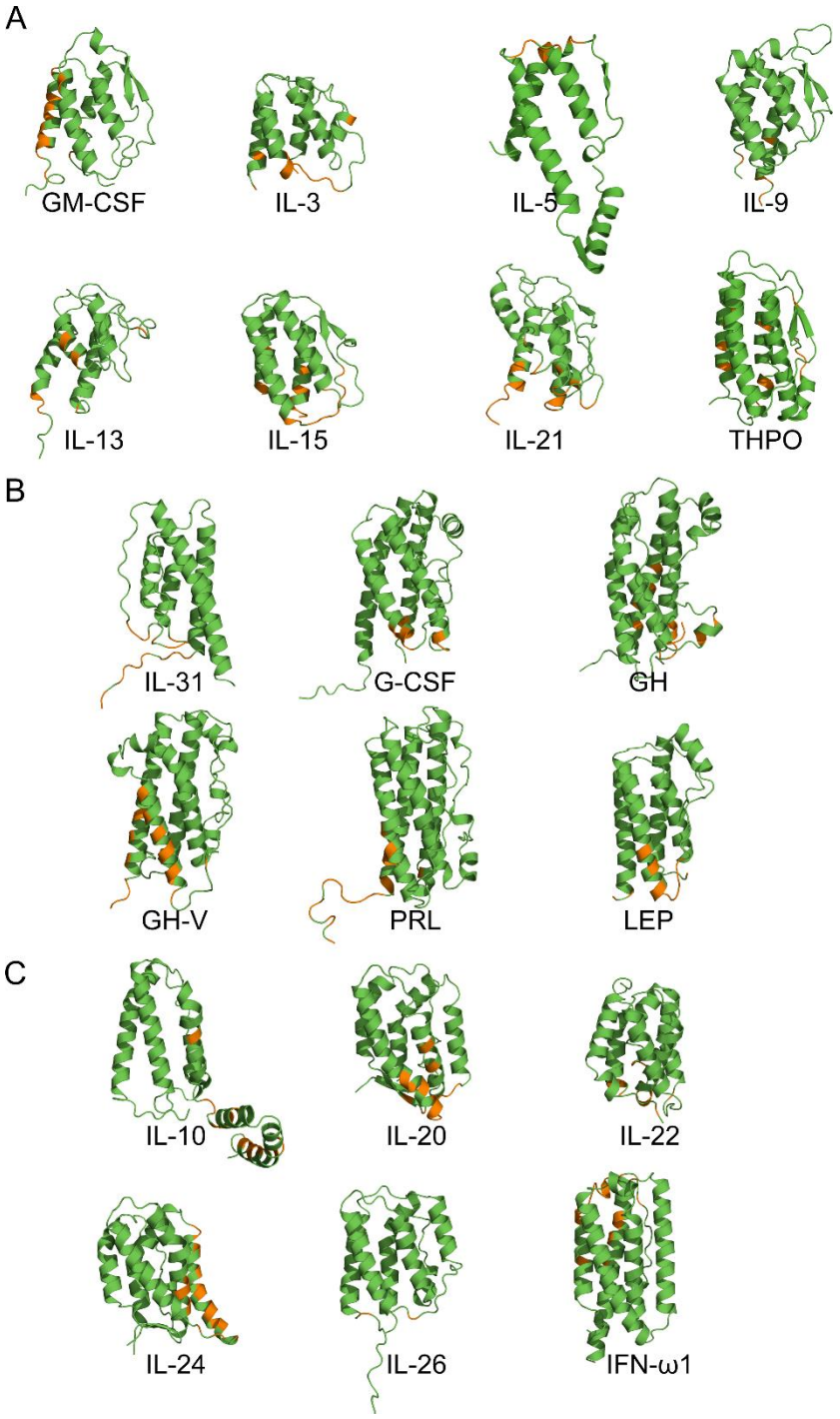

Figure 6. The tertiary structures of the four-helical cytokines of short-chain (panel **A**), long-chain (**B**) and interferons/IL-10 (**C**) families (**Table S3**) used for the structural modeling of their complexes with Ca^{2+}-loaded S100P dimer by ClusPro docking server [40] (only one subunit is shown for IL-5). The contact residues included into 5 or more docking models were considered as the most probable residues of the binding site (orange-colored). N-terminus is located in the lower left corner for each cytokine.

The predicted residues of the binding sites (included into 5 or more docking models) are shown in **Table S4** and **Figures 5A** and **6**. The S100P residues predicted to be most commonly involved into recognition of the four-helical cytokines studied include (19 cytokines out of 20): E5 of helix α1, Y88 and F89 of helix α4. These residues were previously shown to bind V domain of RAGE (PDB entry 2MJW [30]), and predicted to interact with the short-chain cytokine EPO [22]. Furthermore, the residues Y88 and F89 were predicted to interact with IFN-β [19]. Analysis of the distributions of the predicted contact residues

Preprints (www.preprints.org) | NOT PEER-REVIEWED | Posted: 21 September 2022 doi:10.20944/preprints202209.0319.v1

of S100P dimer over its amino acid sequence within models of S100P complexes with the members of specific families of the four-helical cytokines (**Figure 5B**) reveals that these families demonstrate very similar contact surfaces that include helices α1 and α4, and the 'hinge' region between helices α2 and α3. These S100P regions are united into the well-defined binding site, illustrated in **Figure 5A**. Notably, helices α1 and α4, and 'hinge' of S100 proteins are frequently involved in the target recognition [42]. Namely these elements of S100P's secondary structure are engaged in the interaction with the V domain of RAGE (PDB entry 2MJW [30]). Besides, the 'hinge' and helix α4 were earlier predicted to bind IFN-β [19]. Overall, the structural modelling points out the existence of considerable overlapping of the cytokine-binding site with that established for the RAGE domain.

To validate the modelling results, we have studied by SPR spectroscopy affinity of S100P mutants F89A and Δ42-47 (that lacks PGFLQS sequence in the flexible 'hinge') to 11 S100P-specific four-helical cytokines covering all families of this fold (**Table 4**). Despite absence of dramatic structural consequences of these mutations at the level of stabilities of their secondary, tertiary and quaternary structures (see **Figure S1**), with a few exceptions, the both mutants possess notably suppressed affinities to the cytokines (**Table 4**). The effect is more prominent for Δ42-47 mutant, lacking detectable interaction with nearly all cytokines studied, which implies that the respective K_d values exceed 10^{-4} M. Therefore, the mutagenesis data support involvement of the 'hinge' and residue F89 in the recognition of the most of the cytokines studied.

The long-chain cytokines are predicted to interact with Ca^{2+}-bound S100P dimer via the residues of N-terminus and helices α1 and α3 (**Figure 6B**). The cytokines of interferons/IL-10 family, except for IL-26 with minimal number of the contact residues, are predicted to bind S100P dimer by helices α2 and α3, and some residues of C-terminus (**Figure 6C**). The predicted contact residues of the short-chain cytokines do not reveal evident regularity in their location (**Figure 6A**). Meanwhile, the contact residues of the γ_c family of cytokines (IL-9, IL-15 and IL-21 [43]) are located in the helices α1, α3 and α4, whereas the predicted S100P-binding site of THPO is similar to those of the long-chain cytokines PRL and LEP. Overall, the location of the predicted S100P-binding surfaces in the four-helical cytokines is variable and cytokine-dependent.

Analysis of the cytokine tertiary structures in the complexes of some of the S100P-specific cytokines with their respective receptors shows partial overlapping of the receptor-binding sites with the predicted S100P-binding sites (**Table S4**). Hence, S100P binding should interfere with the formation of the cytokine-receptor complexes. This conclusion is in line with the previous data on the inhibition of IFN-β signaling in MCF-7 cells by S100A1/A4/B/P [10,19,20].

It should be emphasized, that the accuracy of the predictions of tertiary structures of the S100P-cytokine complexes based upon molecular docking is limited, since they do not take into consideration structural flexibility of the interaction partners. This is especially true in the case of the presence of the regions prone to disordering, including S100P (PDB entry 1J55 contains unresolved fragment 46-51), IL-15 (2Z3Q: unresolved fragment 76-80), THPO (1V7M, 1V7N: ~163 from 332 residues are ordered), G-CSF (DisProt [44] entry DP03184), LEP (1AX8: unresolved fragment 25-38), IL-10 (2ILK: unresolved fragment 1-5). This is further illustrated by **Figure 7** showing that all four-helical cytokines analyzed in this study are characterized by the noticeable levels of predicted intrinsic disorder, indicating that the abundantly present structural flexibility is likely to play important roles in their functionality.

Preprints (www.preprints.org) | NOT PEER-REVIEWED | Posted: 21 September 2022 doi:10.20944/preprints202209.0319.v1

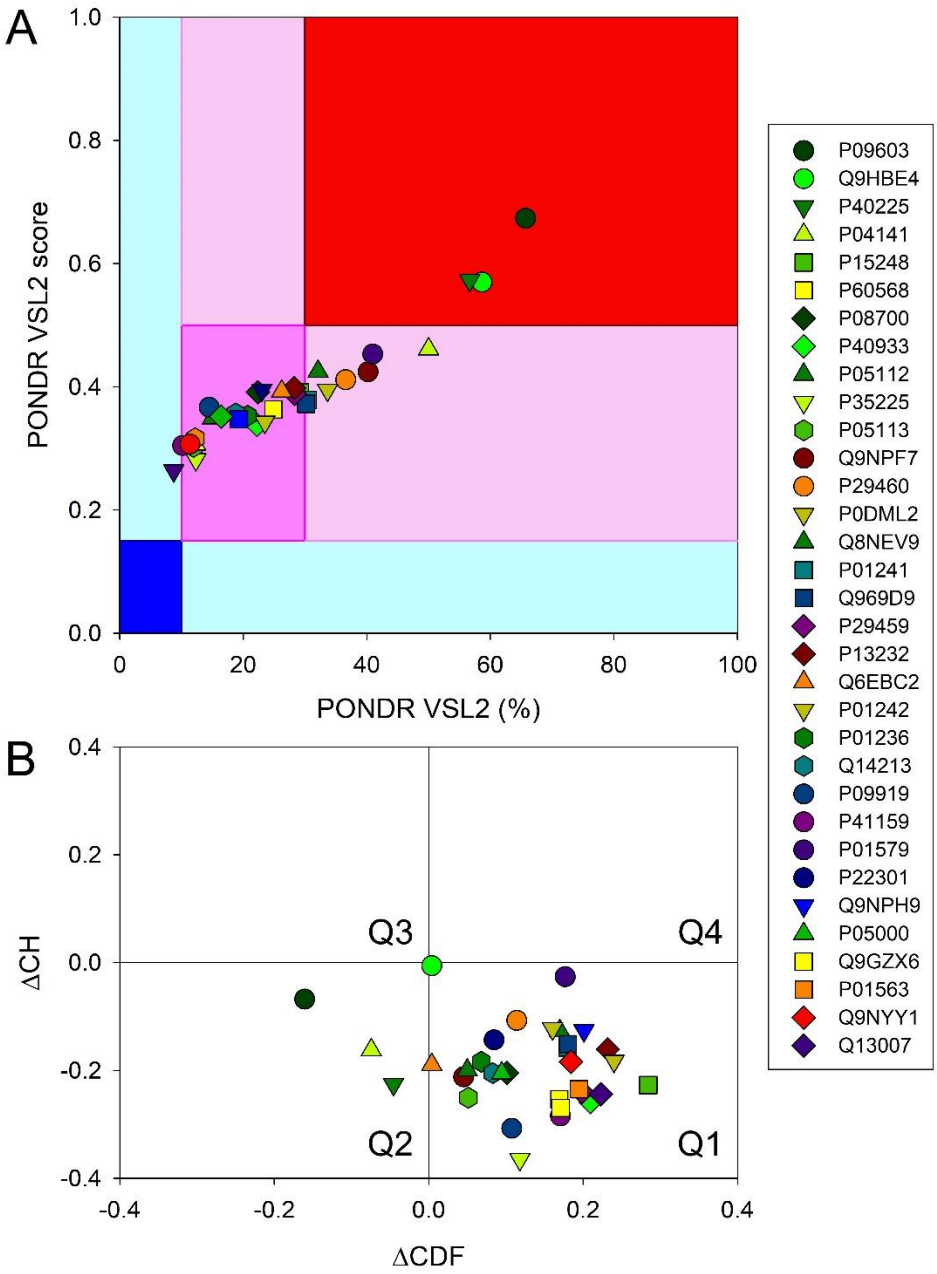

Figure 7. Global intrinsic disorder analysis of the human four-helical cytokines. A. The PONDR® VSL2 output, where the PONDR® VSL2 score is the average disorder score of a query protein, and PONDR® VSL2 (%) is a percent of the predicted disordered residues with the disorder scores above 0.5. Color blocks indicate regions in which proteins are mostly ordered (blue and light blue), moderately disordered (pink and light pink), or mostly disordered (red). If the two parameters agree, the corresponding part of background is dark (blue, pink, or red), whereas light blue and light pink reflect areas in which only one of these criteria applies. B. CH-CDF plot combining outputs of the charge-hydropathy (CH) and cumulative distribution function (CDF) analyses. The Y-coordinate is calculated as the distance of the corresponding protein from the boundary in the CH plot. The X-coordinate is calculated as the average distance of the corresponding protein's CDF curve from the CDF boundary. The quadrant that the protein is located determines its disorder-based classification: Q1, protein predicted to be ordered by both tools (i.e., mostly ordered proteins); Q2, protein predicted to be ordered by CH-plot and disordered by CDF (i.e., native molten globules); Q3, protein predicted to be disordered by both tools (i.e., mostly disordered proteins); Q4, protein predicted to be disordered by CH-plot and ordered by CDF.

3. Materials and methods

Preprints (www.preprints.org) | NOT PEER-REVIEWED | Posted: 21 September 2022 doi:10.20944/preprints202209.0319.v1

3.1. Materials

Human S100P protein and its F89A and Δ42-47 (lacks PGFLQS sequence) mutants were prepared in *E. coli* as previously described [28]. The cytokine samples used in the present work are listed in **Table 2**. Protein concentrations were measured spectrophotometrically using extinction coefficients at 280 nm calculated according to ref. [45].

Sodium acetate and ethanolamine were bought from Bio-Rad Laboratories, Inc. HEPES, sodium chloride and SDS were from PanReac AppliChem. Potassium hydroxide, $CaCl_2$, EDTA and TWEEN 20 were purchased from Sigma Aldrich Co. Tricine was from Helicon (Moscow, Russia). Glutaraldehyde was from Amersham Biosciences. Coomassie brilliant blue R-250 was bought from Merck.

3.2. Surface plasmon resonance studies

Surface plasmon resonance (SPR) measurements of S100P affinity to cytokines at 25°C were performed using ProteOn™ XPR36 protein interaction array system (Bio-Rad Laboratories, Inc.). Ligand (0.03 mg/ml cytokine) in 10 mM sodium acetate pH 4.5 buffer was immobilized on ProteOn™ GLH sensor chip surface (up to 9,000-14,000 RUs) by amine coupling, according to the manufacturer's instructions. The remaining activated amine groups on the chip surface were blocked by 1 M ethanolamine solution. Analyte (62 nM - 16 μM S100P) in a running buffer (10 mM HEPES, 150 mM NaCl, 1 mM $CaCl_2$, 0.05% TWEEN 20, pH 7.4) was passed over the chip surface at a rate of 30 μl/min for 300 s, followed by flushing the chip with the running buffer for 2,400 s. Each double-referenced SPR sensogram was fitted according to either a one-site binding model (S100P - IL-13 interaction) or a *heterogeneous ligand* model (1), which assumes existence of two populations of the ligand (L_1 and L_2) that bind a single analyte molecule (A):

$$L_1 + A \underset{k_{d1}}{\overset{k_{a1}}{\rightleftarrows}} L_1A \qquad L_2 + A \underset{k_{d2}}{\overset{k_{a2}}{\rightleftarrows}} L_2A \qquad (1)$$

$$K_{d1} \qquad K_{d2}$$

where k_a and k_d refer to kinetic association and dissociation constants, respectively, while K_d are equilibrium dissociation constants (k_d/k_a). K_d and k_d values were evaluated for each analyte concentration using ProteOn Manager™ v.3.1 software (Bio-Rad Laboratories, Inc.), followed by averaging of the resulting values (n = 3-5). The standard deviations are indicated. The ligand was regenerated by passage of 20 mM EDTA solution pH 8.0 for 100 s. The free energy changes, accompanying the interaction between S100P and the cytokines were calculated as follows: $\Delta G_i = - RT \ln(55.3/K_{di})$, i=1,2.

3.3. Structural classification of cytokines

The cytokines were structurally classified according to the SCOP 2 database, build 1.0.6, updated on 06-29-2022 (https://scop2.mrc-lmb.cam.ac.uk [27]). The cytokines studied belong to the "All alpha proteins" structural class, "4-helical cytokines" fold (SCOP ID 2001054; core: 4 helices, bundle, closed, left-handed twist, 2 crossover connections), "4-helical cytokines" superfamily (SCOP ID 3001717). The superfamily contains the following families: "Long-chain cytokines" (SCOP ID 4000851), "Short-chain cytokines" (SCOP ID 4000852) and "Interferons/interleukin-10 (IL-10)" (SCOP ID 4000854).

3.4. Modeling of the S100P-cytokine complexes

The models of tertiary structures of S100P-cytokine complexes were built using ClusPro docking server [40] mainly as previously described [22]. The structure of Ca2+-loaded human S100P dimer was extracted from the structure of its complex with V domain of RAGE (chains B, D of PDB [46] entry 2MJW). The tertiary structures of human cytokines have been taken from PDB or predicted using AlphaFold2 (https://alphafold.ebi.ac.uk/ [41]) (**Table S3**). The signal peptides were excluded from the protein amino acid sequences for the predictions. In the case of the presence of unresolved regions

Preprints (www.preprints.org) | NOT PEER-REVIEWED | Posted: 21 September 2022 doi:10.20944/preprints202209.0319.v1

in PDB structures of the proteins, their full-length structures were taken from tertiary structures of the proteins in complex with their binding partners. Distributions of the contact residues in the docking models over the protein sequences were calculated as described in ref. [22]. The contact residues included into 5 or more docking models were considered as the most probable residues of the binding site (numbering is according to the PDB entries). For distributions of the contact residues of Ca2+-loaded S100P dimer over its amino acid sequence within models of S100P complexes with representatives of specific families of four-helical cytokines 10 docking models were taken into account for each S100P-cytokine pair. The tertiary structures were drawn with molecular graphics system PyMOL v.2.5.0 (https://pymol.org/2/).

3.5. Comparison of structural properties of WT S100P and its mutants

Calcium removal from S100P samples was performed according to ref. [47]. Buffer conditions: 10 mM tricine-KOH, 1 mM EDTA-KOH, pH 7.4.

CD spectra of S100P samples (10 μM) were measured at 20ºC using JASCO J-810 spectropolarimeter (JASCO Inc., Japan), equipped with a Peltier-controlled cell holder (quartz cell with optical path length of 1 mm). The instrument was calibrated according to the manufacturer's instruction. Bandwidth was 2 nm, averaging time 2 s, and accumulation 3. The spectral contribution of the buffer was subtracted from the protein spectra.

Fluorescence spectra of S100P samples (10 μM) were measured using Cary Eclipse spectrometer (Varian Inc.), equipped with a Peltier-controlled cell holder (10×10 mm quartz cell). The sample temperature was monitored inside the cell. Fluorescence of S100P was excited at 280 nm; excitation and emission bandwidths were 5 nm; photomultiplier voltage of 800 V. Scanning of emission wavelengths from 290 nm to 380 nm, step 2 nm, averaging time 1 s. The emission spectra were corrected for spectral sensitivity of the spectrometer and described by a log-normal function [48] using LogNormal software (IBI RAS, Pushchino, Russia). The fluorescence emission maximum positions, λmax, were estimated from these fits. The temperature scans were performed stepwise upon heating, allowing the sample to equilibrate at each temperature for 3 min; average heating rate of 0.5 °C/min.

Crosslinking of decalcified S100P (67 μM) with 0.02% glutaraldehyde was performed at 20ºC for 16 h. The reaction was quenched by addition of SDS sample buffer. The resulting sample was analyzed by SDS–PAGE using 18% resolving gel, 5 μg of protein per lane [49]. The gels were stained with Coomassie brilliant blue R-250 and scanned using Molecular Imager PharosFX Plus System (Bio-Rad Laboratories, Inc.). The quantitation of each band was performed using Quantity One software.

3.6. Intrinsic disorder analysis of human four-helical cytokines

Intrinsic disorder propensities of human four-helical cytokines were evaluated by the PONDR® VSL2 computational tool, which combines neural network predictors for short and long disordered regions [50] and which is one of the more accurate stand-alone disorder predictors [51-53]. To evaluate global disorder predisposition of a query protein, we calculated the percent of predicted disordered residues (i.e., residues with the disorder scores above 0.5) and also calculated the average disorder score as a protein length-normalized sum of all the per-residue disorder scores in a query protein.

Important information on the global classification of disorder status of query proteins can be obtained using binary disorder predictors (i.e., computational tools that classify proteins as wholly ordered or wholly disordered), such as the charge-hydropathy (CH) plot [54,55] and the cumulative distribution function (CDF) plot [55,56]. CH-plot utilizes information on the absolute mean net charge and mean hydropathy to classify query proteins as proteins with substantial amounts of extended disorder (native coils and native pre-molten globules) or proteins with compact globular conformations (native molten globules and ordered proteins) [55,57]. CDF analysis uses the PONDR outputs to discriminate all types of disorder (native coils, native molten globules and native pre-molten globules) from ordered proteins [55]. As a result, the combined CH-CDF plot gives an opportunity for unique assessment of intrinsic disorder in several categories, providing a means

 doi:10.20944/preprints202209.0319.v1

for predictive classification of proteins into structurally different classes [56,58,59]. To generate a corresponding CH-CDF plot, the coordinates of a query protein are calculated as a distance from the boundary in the CH-plot (Y-coordinate) and an average distance of the respective CDF curve from the CDF boundary (X-coordinate). Proteins are then classified based on their positions within the quadrants of the CH-CDF plot. Here, the lower-right quadrant (Q1) includes ordered proteins (i.e., those predicted as ordered and compact by both CDF and CH); the lower-left quadrant (Q2) contains proteins predicted to be disordered by CDF but compact by CH-plot (i.e., native molten globules or hybrid proteins containing sizable levels of order and disorder); the upper-left quadrant (Q3) contains proteins predicted to be disordered by both methods (i.e., proteins with extended disorder, such as native coils and native pre-molten globules); and the upper-right quadrant (Q4) contains proteins predicted to be disordered by CH-plot but ordered by CDF [58].

4. Conclusions

Among the 41 four-helical cytokines studied to date with regard to their affinity to S100P protein (**Tables 1**, **2**, and **S1**) only 12 cytokines did not reveal specificity to S100P (**Table S1**). Thus, ca 71% of the four-helical cytokines exhibit affinity to Ca2+-bound S100P dimer exceeding that for the V domain of its receptor, RAGE (**Tables 1**, and **3**). Since except for the GH - GH-V pair the S100P-specific cytokines are evolutionary distant from each other, the S100P-cytokine interactions are mostly non-redundant. Considering that the S100P monomerization is expected to favor its interaction with the four-helical cytokines, the fraction of the S100P-specific cytokines is likely to be even higher. Therefore, S100P represents a unique case of the promiscuous binding partner for the most of four-helical cytokines. The molecular docking and the mutagenesis study point out some structural basics of this phenomenon. The cytokine-binding sites of S100P protein seem to overlap with its RAGE-binding site, and include residues of helices α1 and α4, and the 'hinge' region (**Figure 5**). Meanwhile, regularities of the location of S100P-binding sites of the cytokines remain fairly enigmatic (**Figure 6**). Nevertheless, in some cases these sites seem to overlap with the known receptor-binding sites of the cytokines (**Table S4**), thereby indicating that binding of the extracellular S100P should interfere with their signaling. Binding of some of the cytokines to S100P is potentially able to modulate its signaling, especially under the pathological conditions accompanied by an increase in concentrations of the cytokines. Binding of the intracellular S100P could promote non-canonical secretion of the S100P-specific cytokines, similarly to the several reported cases [24,25,39]. Finally, quantitative excess of S100P protein suggests that it could serve as a buffer for the multiple four-helical cytokines, stabilizing their free concentrations.

S100P is considered as one of the most promiscuous members of S100 protein family, able to bind numerous ligands with a high affinity, and sharing interaction partners with other S100 proteins [60,61]. Therefore, one may expect that other representatives of the S100 protein family are cross-reactive with the same four-helical cytokines, as previously shown for IL-6 family [21]. Further studies should verify this hypothesis, provide more molecular details of the S100-cytokine interactions, give us a clue for better understanding of the structural basics of their selectivity, and establish their functional significance.

Abbreviations: CDF, cummulative distribution function; CH, charge-hydropathy; CHO, Chinese hamster ovary cells; EDTA, ethylenediaminetetraacetic acid; EPO, erythropoietin; FGF, fibroblast growth factor; HEK293, Human embryonic kidney 293 cells; HEPES, 4-(2-hydroxyethyl)piperazine-1-ethanesulfonic acid; G-CSF, granulocyte colony-stimulating factor; GH, Growth hormone/somatotropin; GH-V, growth hormone variant; GM-CSF, granulocyte-macrophage colony-stimulating factor; IFN, interferon; IL, interleukin; LEP, leptin; M-CSF, macrophage colony-stimulating factor 1; NMR, nuclear magnetic resonance; PDB, Protein Data Bank; PL, chorionic somatomammotropin hormone 1; PRL, prolactin; RAGE, receptor for advanced glycation end products; SCOP, Structural Classification of Proteins; SDS–PAGE, sodium dodecyl sulfate–polyacrylamide gel electrophoresis; SPR, surface plasmon resonance; RU, resonance unit; THPO, thrombopoietin; TSLP, thymic stromal

lymphopoietin; Δ42-47, human S100P mutant lacking PGFLQS sequence in the 'hinge' region; WT, wild-type protein

Supplementary Materials: The following supporting information can be downloaded at: www.mdpi.com/xxx/s1, Figure S1: Comparison of structural properties of apo-forms of WT S100P and its F89A, Δ42-47 mutants, using far-UV CD spectroscopy at 20ºC (panel A), intrinsic fluorescence (B) and chemical crosslinking at 20ºC by 0.02% glutaraldehyde for 16 h (C) (10 mM tricine-KOH, 1 mM EDTA-KOH, pH 7.4); Table S1: The four-helical cytokine samples that did not reveal specificity to S100P, according to SPR spectroscopy (cytokine immobilization on the sensor chip surface by amine coupling);Table S2: The concentrations of four-helical cytokines under normal and pathological conditions; Table S3: The structures (PDB entries or AlphaFold2 predictions) of the human cytokines used for structural modelling of their complexes with Ca2+-loaded human S100P dimer (chains B, D of PDB entry 2MJW) using ClusPro docking server; Table S4: The residues of the binding sites for the S100P-cytokine complexes predicted using ClusPro docking server.

Author Contributions: Conceptualization, S.E.P.; methodology, A.S.K., E.I.D., and V.N.U.; validation, A.S.K., E.I.D., V.N.U., and S.E.P.; formal analysis, A.S.K., E.I.D., V.N.U., and S.E.P.; investigation, A.S.K., E.I.D., M.E.P., A.S.S., V.A.R., V.N.U., and S.E.P.; resources, S.E.P.; data curation, A.S.K., E.I.D., V.A.R., V.N.U., and S.E.P.; writing—original draft preparation, A.S.K., E.I.D., V.A.R., V.N.U., and S.E.P.; writing—review and editing, V.N.U., E.A.P., and S.E.P.; visualization, A.S.K., E.I.D., V.N.U., and S.E.P.; supervision, E.A.P. and S.E.P.; project administration, S.E.P.; funding acquisition, S.E.P. All authors have read and agreed to the published version of the manuscript.

Funding: This research was funded by a grant to S.E.P. from the Russian Science Foundation (№19-14-00289-П).

Institutional Review Board Statement: Not applicable.

Informed Consent Statement: Not applicable.

Data Availability Statement: In this section, please provide details regarding where data supporting reported results can be found, including links to publicly archived datasets analyzed or generated during the study. Please refer to suggested Data Availability Statements in section "MDPI Research Data Policies" at https://www.mdpi.com/ethics. If the study did not report any data, you might add "Not applicable" here.

Conflicts of Interest: The authors declare no conflict of interest. The funders had no role in the design of the study; in the collection, analyses, or interpretation of data; in the writing of the manuscript, or in the decision to publish the results.

References

1. Donato, R.; Cannon, B.R.; Sorci, G.; Riuzzi, F.; Hsu, K.; Weber, D.J.; Geczy, C.L. Functions of S100 Proteins. *Curr Mol Med* **2013**, *13*, 24-57.
2. Sreejit, G.; Flynn, M.C.; Patil, M.; Krishnamurthy, P.; Murphy, A.J.; Nagareddy, P.R. S100 family proteins in inflammation and beyond. *Adv Clin Chem* **2020**, *98*, 173-231, doi:10.1016/bs.acc.2020.02.006.
3. Singh, P.; Ali, S.A. Multifunctional Role of S100 Protein Family in the Immune System: An Update. *Cells* **2022**, *11*, doi:10.3390/cells11152274.
4. Nockolds, C.E.; Kretsinger, R.H.; Coffee, C.J.; Bradshaw, R.A. Structure of a calcium-binding carp myogen. *Proc.Natl.Acad.Sci.U.S.A* **1972**, *69*, 581-584.
5. Sigrist, C.J.; de Castro, E.; Cerutti, L.; Cuche, B.A.; Hulo, N.; Bridge, A.; Bougueleret, L.; Xenarios, I. New and continuing developments at PROSITE. *Nucleic Acids Res* **2013**, *41*, D344-347, doi:10.1093/nar/gks1067.
6. Zimmer, D.B.; Eubanks, J.O.; Ramakrishnan, D.; Criscitiello, M.F. Evolution of the S100 family of calcium sensor proteins. *Cell Calcium* **2013**, *53*, 170-179, doi:10.1016/j.ceca.2012.11.006.
7. Fritz, G.; Heizmann, C.W. 3D Structures of the Calcium and Zinc Binding S100 Proteins. In *Handbook of Metalloproteins*, John Wiley & Sons, L., Ed. 2004; 10.1002/0470028637.met046.
8. Streicher, W.W.; Lopez, M.M.; Makhatadze, G.I. Modulation of quaternary structure of S100 proteins by calcium ions. *Biophys Chem* **2010**, *151*, 181-186, doi:10.1016/j.bpc.2010.06.003.

9. Gilston, B.A.; Skaar, E.P.; Chazin, W.J. Binding of transition metals to S100 proteins. *Sci China Life Sci* **2016**, *59*, 792-801, doi:10.1007/s11427-016-5088-4.
10. Kazakov, A.S.; Mayorov, S.A.; Deryusheva, E.I.; Avkhacheva, N.V.; Denessiouk, K.A.; Denesyuk, A.I.; Rastrygina, V.A.; Permyakov, E.A.; Permyakov, S.E. Highly specific interaction of monomeric S100P protein with interferon beta. *Int J Biol Macromol* **2020**, *143*, 633-639, doi:10.1016/j.ijbiomac.2019.12.039.
11. Bresnick, A.R.; Weber, D.J.; Zimmer, D.B. S100 proteins in cancer. *Nat Rev Cancer* **2015**, *15*, 96-109, doi:10.1038/nrc3893.
12. Cristóvão, J.S.; Gomes, C.M. S100 Proteins in Alzheimer's Disease. *Front Neurosci-Switz* **2019**, *13*, 463, doi:10.3389/Fnins.2019.00463.
13. Holzinger, D.; Tenbrock, K.; Roth, J. Alarmins of the S100-Family in Juvenile Autoimmune and Auto-Inflammatory Diseases. *Front Immunol* **2019**, *10*, 182-182, doi:10.3389/fimmu.2019.00182.
14. Sattar, Z.; Lora, A.; Jundi, B.; Railwah, C.; Geraghty, P. The S100 Protein Family as Players and Therapeutic Targets in Pulmonary Diseases. *Pulm Med* **2021**, *2021*, 5488591, doi:10.1155/2021/5488591.
15. Gonzalez, L.L.; Garrie, K.; Turner, M.D. Role of S100 proteins in health and disease. *Biochim Biophys Acta Mol Cell Res* **2020**, *1867*, 118677, doi:10.1016/j.bbamcr.2020.118677.
16. Allgower, C.; Kretz, A.L.; von Karstedt, S.; Wittau, M.; Henne-Bruns, D.; Lemke, J. Friend or Foe: S100 Proteins in Cancer. *Cancers (Basel)* **2020**, *12*, doi:10.3390/cancers12082037.
17. Bresnick, A.R. S100 proteins as therapeutic targets. *Biophys Rev* **2018**, *10*, 1617-1629, doi:10.1007/s12551-018-0471-y.
18. Rumpret, M.; von Richthofen, H.J.; van der Linden, M.; Westerlaken, G.H.A.; Talavera Ormeno, C.; Low, T.Y.; Ovaa, H.; Meyaard, L. Recognition of S100 proteins by Signal Inhibitory Receptor on Leukocytes-1 negatively regulates human neutrophils. *Eur J Immunol* **2021**, *51*, 2210-2217, doi:10.1002/eji.202149278.
19. Kazakov, A.S.; Sofin, A.D.; Avkhacheva, N.V.; Denesyuk, A.I.; Deryusheva, E.I.; Rastrygina, V.A.; Sokolov, A.S.; Permyakova, M.E.; Litus, E.A.; Uversky, V.N., et al. Interferon Beta Activity Is Modulated via Binding of Specific S100 Proteins. *Int J Mol Sci* **2020**, *21*, doi:10.3390/ijms21249473.
20. Kazakov, A.S.; Sofin, A.D.; Avkhacheva, N.V.; Deryusheva, E.I.; Rastrygina, V.A.; Permyakova, M.E.; Uversky, V.N.; Permyakov, E.A.; Permyakov, S.E. Interferon-β Activity Is Affected by S100B Protein. *Int J Mol Sci* **2022**, *23*, doi:10.3390/ijms23041997.
21. Kazakov, A.S.; Sokolov, A.S.; Permyakova, M.E.; Litus, E.A.; Uversky, V.N.; Permyakov, E.A.; Permyakov, S.E. Specific cytokines of interleukin-6 family interact with S100 proteins. *Cell Calcium* **2022**, *101*, 102520, doi:10.1016/j.ceca.2021.102520.
22. Kazakov, A.S.; Deryusheva, E.I.; Sokolov, A.S.; Permyakova, M.E.; Litus, E.A.; Rastrygina, V.A.; Uversky, V.N.; Permyakov, E.A.; Permyakov, S.E. Erythropoietin Interacts with Specific S100 Proteins. *Biomolecules* **2022**, *12*, doi:10.3390/biom12010120.
23. Klingelhofer, J.; Moller, H.D.; Sumer, E.U.; Berg, C.H.; Poulsen, M.; Kiryushko, D.; Soroka, V.; Ambartsumian, N.; Grigorian, M.; Lukanidin, E.M. Epidermal growth factor receptor ligands as new extracellular targets for the metastasis-promoting S100A4 protein. *Febs J* **2009**, *276*, 5936-5948, doi:10.1111/j.1742-4658.2009.07274.x.
24. Mohan, S.K.; Yu, C. The IL1alpha-S100A13 heterotetrameric complex structure: a component in the non-classical pathway for interleukin 1alpha secretion. *J Biol Chem* **2011**, *286*, 14608-14617, doi:10.1074/jbc.M110.201954.
25. Carreira, C.M.; LaVallee, T.M.; Tarantini, F.; Jackson, A.; Lathrop, J.T.; Hampton, B.; Burgess, W.H.; Maciag, T. S100A13 is involved in the regulation of fibroblast growth factor-1 and p40 synaptotagmin-1 release in vitro. *Journal of Biological Chemistry* **1998**, *273*, 22224-22231, doi:10.1074/jbc.273.35.22224.
26. Gupta, A.A.; Chou, R.H.; Li, H.C.; Yang, L.W.; Yu, C. Structural insights into the interaction of human S100B and basic fibroblast growth factor (FGF2): Effects on FGFR1 receptor signaling. *Bba-Proteins Proteom* **2013**, *1834*, 2606-2619, doi:10.1016/j.bbapap.2013.09.012.
27. Andreeva, A.; Kulesha, E.; Gough, J.; Murzin, A.G. The SCOP database in 2020: expanded classification of representative family and superfamily domains of known protein structures. *Nucleic Acids Res* **2020**, *48*, D376-D382, doi:10.1093/nar/gkz1064.

28. Kazakov, A.S.; Sokolov, A.S.; Rastrygina, V.A.; Solovyev, V.V.; Ismailov, R.G.; Mikhailov, R.V.; Ulitin, A.B.; Yakovenko, A.R.; Mirzabekov, T.A.; Permyakov, E.A., et al. High-affinity interaction between interleukin-11 and S100P protein. *Biochem Biophys Res Commun* **2015**, *468*, 733-738, doi:10.1016/j.bbrc.2015.11.024.
29. Kazakov, A.S.; Sokolov, A.S.; Vologzhannikova, A.A.; Permyakova, M.E.; Khorn, P.A.; Ismailov, R.G.; Denessiouk, K.A.; Denesyuk, A.I.; Rastrygina, V.A.; Baksheeva, V.E., et al. Interleukin-11 binds specific EF-hand proteins via their conserved structural motifs. *J Biomol Struct Dyn* **2017**, *35*, 78-91, doi:10.1080/07391102.2015.1132392.
30. Penumutchu, S.R.; Chou, R.H.; Yu, C. Structural Insights into Calcium-Bound S100P and the V Domain of the RAGE Complex. *Plos One* **2014**, *9*, e103947, doi:10.1371/journal.pone.0103947.
31. Orchard, S.; Ammari, M.; Aranda, B.; Breuza, L.; Briganti, L.; Broackes-Carter, F.; Campbell, N.H.; Chavali, G.; Chen, C.; del-Toro, N., et al. The MIntAct project--IntAct as a common curation platform for 11 molecular interaction databases. *Nucleic Acids Res* **2014**, *42*, D358-363, doi:10.1093/nar/gkt1115.
32. Oughtred, R.; Rust, J.; Chang, C.; Breitkreutz, B.J.; Stark, C.; Willems, A.; Boucher, L.; Leung, G.; Kolas, N.; Zhang, F., et al. The BioGRID database: A comprehensive biomedical resource of curated protein, genetic, and chemical interactions. *Protein Sci* **2021**, *30*, 187-200, doi:10.1002/pro.3978.
33. Madeira, F.; Park, Y.M.; Lee, J.; Buso, N.; Gur, T.; Madhusoodanan, N.; Basutkar, P.; Tivey, A.R.N.; Potter, S.C.; Finn, R.D., et al. The EMBL-EBI search and sequence analysis tools APIs in 2019. *Nucleic Acids Res* **2019**, *47*, W636-W641, doi:10.1093/nar/gkz268.
34. Lee, Y.C.; Volk, D.E.; Thiviyanathan, V.; Kleerekoper, Q.; Gribenko, A.V.; Zhang, S.M.; Gorenstein, D.G.; Makhatadze, G.I.; Luxon, B.A. Letter to the Editor: NMR structure of the Apo-S100P protein. *J Biomol Nmr* **2004**, *29*, 399-402, doi:10.1023/B:Jnmr.0000032617.88899.4b.
35. Zhang, H.; Wang, G.; Ding, Y.; Wang, Z.; Barraclough, R.; Rudland, P.S.; Fernig, D.G.; Rao, Z. The crystal structure at 2A resolution of the Ca2+ -binding protein S100P. *J Mol Biol* **2003**, *325*, 785-794.
36. Wu, Z.; Boonmars, T.; Nagano, I.; Boonjaraspinyo, S.; Srinontong, P.; Ratasuwan, P.; Narong, K.; Nielsen, P.S.; Maekawa, Y. Significance of S100P as a biomarker in diagnosis, prognosis and therapy of opisthorchiasis-associated cholangiocarcinoma. *Int J Cancer* **2016**, *138*, 396-408, doi:10.1002/ijc.29721.
37. Permyakov, S.E.; Denesyuk, A.I.; Denessiouk, K.A.; Permyakova, M.E.; Kazakov, A.S.; Ismailov, R.G.; Rastrygina, V.A.; Sokolov, A.S.; Permyakov, E.A. Monomeric state of S100P protein: Experimental and molecular dynamics study. *Cell Calcium* **2019**, *80*, 152-159, doi:10.1016/j.ceca.2019.04.008.
38. Spadaro, A.; Rinaldi, T.; Riccieri, V.; Valesini, G.; Taccari, E. Interleukin 13 in synovial fluid and serum of patients with psoriatic arthritis. *Ann Rheum Dis* **2002**, *61*, 174-176, doi:10.1136/ard.61.2.174.
39. Rousseau, F.; Gauchat, J.F.; McLeod, J.G.; Chevalier, S.; Guillet, C.; Guilhot, F.; Cognet, I.; Froger, J.; Hahn, A.F.; Knappskog, P.M., et al. Inactivation of cardiotrophin-like cytokine, a second ligand for ciliary neurotrophic factor receptor, leads to cold-induced sweating syndrome in a patient. *Proc Natl Acad Sci U S A* **2006**, *103*, 10068-10073, doi:10.1073/pnas.0509598103.
40. Desta, I.T.; Porter, K.A.; Xia, B.; Kozakov, D.; Vajda, S. Performance and Its Limits in Rigid Body Protein-Protein Docking. *Structure* **2020**, *28*, 1071-1081 e1073, doi:10.1016/j.str.2020.06.006.
41. Jumper, J.; Evans, R.; Pritzel, A.; Green, T.; Figurnov, M.; Ronneberger, O.; Tunyasuvunakool, K.; Bates, R.; Zidek, A.; Potapenko, A., et al. Highly accurate protein structure prediction with AlphaFold. *Nature* **2021**, *596*, 583-589, doi:10.1038/s41586-021-03819-2.
42. Permyakov, S.E.; Ismailov, R.G.; Xue, B.; Denesyuk, A.I.; Uversky, V.N.; Permyakov, E.A. Intrinsic disorder in S100 proteins. *Mol Biosyst* **2011**, *7*, 2164-2180, doi:10.1039/c0mb00305k.
43. Leonard, W.J.; Lin, J.X.; O'Shea, J.J. The gammac Family of Cytokines: Basic Biology to Therapeutic Ramifications. *Immunity* **2019**, *50*, 832-850, doi:10.1016/j.immuni.2019.03.028.

44. Quaglia, F.; Meszaros, B.; Salladini, E.; Hatos, A.; Pancsa, R.; Chemes, L.B.; Pajkos, M.; Lazar, T.; Pena-Diaz, S.; Santos, J., et al. DisProt in 2022: improved quality and accessibility of protein intrinsic disorder annotation. *Nucleic Acids Res* **2022**, *50*, D480-D487, doi:10.1093/nar/gkab1082.
45. Pace, C.N.; Vajdos, F.; Fee, L.; Grimsley, G.; Gray, T. How to measure and predict the molar absorption coefficient of a protein. *Protein Sci.* **1995**, *4*, 2411-2423.
46. Berman, H.M.; Westbrook, J.; Feng, Z.; Gilliland, G.; Bhat, T.N.; Weissig, H.; Shindyalov, I.N.; Bourne, P.E. The Protein Data Bank. *Nucleic Acids Res.* **2000**, *28*, 235-242.
47. Blum, H.E.; Lehky, P.; Kohler, L.; Stein, E.A.; Fischer, E.H. Comparative properties of vertebrate parvalbumins. *J.Biol.Chem.* **1977**, *252*, 2834-2838.
48. Burstein, E.A.; Emelyanenko, V.I. Log-normal description of fluorescence spectra of organic fluorophores. *Photochem.Photobiol.* **1996**, *64*, 316- 320
49. Schägger, H.; von Jagow, G. Tricine-sodium dodecyl sulfate-polyacrylamide gel electrophoresis for the separation of proteins in the range from 1 to 100 kDa. *Anal Biochem.* **1987**, *166(2)*, 368-379.
50. Peng, K.; Vucetic, S.; Radivojac, P.; Brown, C.J.; Dunker, A.K.; Obradovic, Z. Optimizing long intrinsic disorder predictors with protein evolutionary information. *Journal of bioinformatics and computational biology* **2005**, *3*, 35-60.
51. Peng, Z.L.; Kurgan, L. Comprehensive comparative assessment of in-silico predictors of disordered regions. *Curr Protein Pept Sci* **2012**, *13*, 6-18, doi:10.2174/138920312799277938.
52. Fan, X.; Kurgan, L. Accurate prediction of disorder in protein chains with a comprehensive and empirically designed consensus. *J Biomol Struct Dyn* **2014**, *32*, 448-464, doi:10.1080/07391102.2013.775969.
53. Necci, M.; Piovesan, D.; Predictors, C.; DisProt, C.; Tosatto, S.C.E. Critical assessment of protein intrinsic disorder prediction. *Nat Methods* **2021**, *18*, 472-481, doi:10.1038/s41592-021-01117-3.
54. Uversky, V.N.; Gillespie, J.R.; Fink, A.L. Why are "natively unfolded" proteins unstructured under physiologic conditions? *Proteins* **2000**, *41*, 415-427, doi:10.1002/1097-0134(20001115)41:3<415::aid-prot130>3.0.co;2-7.
55. Oldfield, C.J.; Cheng, Y.; Cortese, M.S.; Brown, C.J.; Uversky, V.N.; Dunker, A.K. Comparing and combining predictors of mostly disordered proteins. *Biochemistry* **2005**, *44*, 1989-2000, doi:10.1021/bi047993o.
56. Xue, B.; Oldfield, C.J.; Dunker, A.K.; Uversky, V.N. CDF it all: consensus prediction of intrinsically disordered proteins based on various cumulative distribution functions. *FEBS Lett* **2009**, *583*, 1469-1474, doi:10.1016/j.febslet.2009.03.070.
57. Huang, F.; Oldfield, C.J.; Xue, B.; Hsu, W.L.; Meng, J.; Liu, X.; Shen, L.; Romero, P.; Uversky, V.N.; Dunker, A. Improving protein order-disorder classification using charge-hydropathy plots. *BMC Bioinformatics* **2014**, *15 Suppl 17*, S4, doi:10.1186/1471-2105-15-S17-S4.
58. Mohan, A.; Sullivan, W.J., Jr.; Radivojac, P.; Dunker, A.K.; Uversky, V.N. Intrinsic disorder in pathogenic and non-pathogenic microbes: discovering and analyzing the unfoldomes of early-branching eukaryotes. *Mol Biosyst* **2008**, *4*, 328-340, doi:10.1039/b719168e.
59. Huang, F.; Oldfield, C.; Meng, J.; Hsu, W.L.; Xue, B.; Uversky, V.N.; Romero, P.; Dunker, A.K. Subclassifying disordered proteins by the CH-CDF plot method. *Pac Symp Biocomput* **2012**, 128-139.
60. Simon, M.A.; Ecsedi, P.; Kovacs, G.M.; Poti, A.L.; Remenyi, A.; Kardos, J.; Gogl, G.; Nyitray, L. High-throughput competitive fluorescence polarization assay reveals functional redundancy in the S100 protein family. *The FEBS journal* **2020**, *287*, 2834-2846, doi:10.1111/febs.15175.
61. Simon, M.A.; Bartus, É.; Mag, B.; Boros, E.; Roszjár, L.; Gógl, G.; Travé, G.; Martinek, T.A.; Nyitray, L. Promiscuity mapping of the S100 protein family using a high-throughput holdup assay. *Sci Rep* **2022**, *12*, 5904, doi:10.1038/s41598-022-09574-2.